Supporting Information

Efficient Co-production of Ammonia and Formic Acid from Nitrate and Polyester via Paired Electrolysis

Mengmeng Du,[‡ a] Tao Sun,[‡ b] Xuyun Guo,[‡ c] Mingzhu Han,[‡ a] Yu Zhang,[a d] Wenxuan Chen,[a] Mengxiang Han,[a] Jizhe Ma,[a] Wenfang Yuan,[a] Chunyu Zhou,[b] Valeria Nicolosi,[c] Jian Shang,[* e] Ning Zhang,[* f, g] and Bocheng Qiu[* a]*

[a] *Jiangsu Key Laboratory of Pesticide Sciences, Department of Chemistry, College of Sciences, Nanjing Agricultural University, Nanjing 210095, China. E-mail: bochengqiu@njau.edu.cn*

[b] *Department of Radiology, Xinqiao Hospital, Army Medical University, Chongqing 400037, China.*

[c] *School of Chemistry, Centre for Research on Adaptive Nanostructures and Nanodevices (CRANN) and Advanced Materials Bio-Engineering Research Centre (AMBER), Trinity College Dublin, Dublin, D02PN40, Ireland.*

[d] *College of Energy and Power Engineering, Nanjing Institute of Technology, Nanjing 211167, China. E-mail: yu_zhang1225@163.com*

[e] *Low-Dimensional Energy Materials Research Center, Shenzhen Institute of Advanced Technology, Chinese Academy of Sciences, Shenzhen 518055, China. E-mail: jian.shang@siat.ac.cn*

[f] *Key Laboratory of Precision and Intelligent Chemistry, Department of Environmental Science and Engineering, University of Science and Technology of China, Hefei, 230026 China. E-mail: zhangning18@ustc.edu.cn*

[g] *Sustainable Energy and Environmental Materials Innovation Center, Suzhou Institute for Advanced Research, University of Science and Technology of China, Suzhou, 215123 China.*

[‡] Mengmeng Du, Tao Sun, Xuyun Guo, and Mingzhu Han contributed equally to this work.

Materials

The commercial nickel foam (NF) mesh was purchased from Lizhiyuan Technology Co., Ltd (Taiyuan, China). This NF features a thickness of 1.7 mm, dimensions of 250 mm × 200 mm, and a pore density of 110 pores per inch. Ammonium fluoride (NH_4F), urea ($CO(NH_2)_2$), nickel chloride hexahydrate ($NiCl_2·6H_2O$), copper chloride ($CuCl_2$), and potassium nitrate (KNO_3) were obtained from Sinopharm Chemical Reagent Co., Ltd. Cobalt nitrate hexahydrate ($Co(NO_3)_3·6H_2O$), potassium hydroxide (KOH), glycolic acid ($C_2H_4O_3$), and formic acid (CH_2O_2) were purchased by Shanghai Aladdin Bio-Chem Technology Co., Ltd. Deionized water (18.25 MΩ cm) was used in all experiments. All the chemicals were used without purification. PET granule was supplied from Shanghai Macklin Biochemical Technology Co., Ltd.

Preparation of Cu-Ni$(OH)_2$/NF

The catalysts were prepared by a hydrothermal method followed by a calculation treatment. Specifically, a commercial Ni foam (NF, 2 × 2.5 cm) was cleaned with 3 M HCl solutions for 5 min under ultrasonic sound conditions, and then washed with deionized (DI) water for three times. Subsequently, the treated nickel foam was immersed in a solution containing NH_4F (3.3 mmol), $CO(NH_2)_2$ (8.3 mmol), $NiCl_2·6H_2O$ (1.5 mmol) and $CuCl_2$ (0.5 mmol). The resulting mixture was then transferred into a Teflon-lined autoclave and heated at 120 °C for 12 h. After cooling down, the Ni foam decorated with Cu-$Ni(OH)_2·xH_2O$ (Cu-$Ni(OH)_2·xH_2O$/NF) was washed with deionized water for several times, and then dried under vacuum. Finally, the Cu-$Ni(OH)_2$ catalyst was obtained by annealing the Cu-$Ni(OH)_2·xH_2O$ precursor at 300 °C for 2 h with a heating rate of 5 °C min^{-1}. To confirm the optimal Cu doping level, the catalysts with other Cu doping contents were obtained by adjusting the $CuCl_2$ addition. Note that the total addition of Ni and Cu precursors was controlled at 2 mmol. The samples with Ni/Cu ratios of 19:1, 9:1, 5:1, 3:1 and 2:1 were synthesized.

Preparation of O_V-Co_3O_4/NF

Typically, 1 mmol $Co(NO_3)_3·6H_2O$, 4 mmol $CO(NH_2)_2$, and 5 mmol NH_4F were dissolved in 40 mL DI water under stirring. A cleaned Ni foam (2 × 2.5 cm) was immersed into the above solution, and then transferred into Teflon-lined autoclave to form Co(OH)F precursors by maintaining at 100 °C for 10 h. Afterwards, the resulting sample was calcined at a muffle

furnace to prepare Co_3O_4/NF. Finally, O_V-Co_3O_4/NF was fabricated from the Co_3O_4/NF through a calculation treatment at 300 ^oC for 1 h in H_2 atmosphere.

Electrochemical procedure

Ethylene glycol (EG) electrooxidation: The electrochemical tests were carried out in a three-electrode system on an electrochemical workstation (Corrtest, CS300MA). The prepared catalyst, Hg/HgO, and carbon rod serve as the working electrode, reference electrode (RE), and counter electrode (CE), respectively. Linear sweep voltammetry (LSV) was performed under 1 M KOH solution containing 0.3 M EG at a scanning rate of 5 mV s^{-1} with 100% *iR* compensation. The *iR* compensation was carried out using the following formula: $E_{corr}=E_{raw}- i\times R_s$, where E_{corr} represents the corrected potential, E_{raw} is the raw potential, i is the current, and R_s is the solution resistance and determined by the electrochemical workstation. The electrochemical surface area (ECSA) measurements were measured in 1 M KOH solution. Electrochemical impedance spectroscopy (EIS) was performed at 0.6 V (vs. Hg/HgO) in the frequency range of 100 kHz to 0.01 Hz. In all tests, the Hg/HgO potential was converted to the reversible hydrogen electrode (RHE) potential using the conversion formula: E (vs. RHE)= E (vs. Hg/HgO)+ 0.0592×pH+ 0.098. The Faradaic efficiency of products (*e.g.*, formic acid (FA) and glycolic acid (GA)) and production rate of FA were calculated as follows:

$$FE_{FA}\ (\%) = \frac{3 \times 96485.3 \times \text{Moles of the obtained FA}}{\text{Totally passed charges}} \times 100\%$$

$$\mathrm{FE}_{GA}(\%) = \frac{4 \times 96485.3 \times \text{Moles of the obtained GA}}{\text{Totally passed charges}} \times 100\%$$

$$\text{FA productivity (mmol } cm^{-2}\, h^{-1}) = \frac{\text{Amount of produced FA (mmol)}}{\text{Area of anode } (cm^2) \times \text{ time (h)}} \times 100\%$$

Nitrate (NO_3^-) electroreduction: Electrochemical experiments were performed on an electrochemical workstation (Corrtest, CS300MA) using an H-type cell with Nafion 117 as the membrane to segregate two chambers. In the NO_3^- reduction reaction system, O_v-Co_3O_4/NF (1 × 1 cm), graphite rod, and Hg/HgO electrode were adopted as working electrode, counter electrode, and reference electrode, respectively. The cathode compartment was filled with 40 mL of electrolyte containing 0.1 M KNO_3 and 1 M KOH. LSV curves were obtained at a scan rate of 5 mV s^{-1} with 100% *iR* compensation. The *iR* compensation was carried

out using the following formula: $E_{corr}=E_{raw}- i\times R_s$, where E_{corr} represents the corrected potential, E_{raw} is the raw potential, i is the current, and R_s is the solution resistance and determined by the electrochemical workstation. ECSA was assessed using CV curves at scan rates ranging from 5 to 25 mV s^{-1} without Faradaic process. The chronoamperometry measurement (i-t curve) was applied at different potentials for 2 h. All potentials were calibrated to the RHE. The Faradaic efficiency of products (*e.g.*, ammonia (NH_3) and nitrite (NO_{2-})) and production rate of NH_3 were calculated as follows:

$$\mathrm{FE}_{NH3}(\%) = \frac{8 \times 96485.3 \times \text{Moles of the obtained } NH_3}{\text{Totally passed charges}} \times 100\%$$

$$\mathrm{FE}_{NO2-}(\%) = \frac{2 \times 96485.3 \times \text{Moles of the obtained } NO_2^-}{\text{Totally passed charges}} \times 100\%$$

$$NH_3 \text{ productivity (mmol } cm^{-2}\, h^{-1}) = \frac{\text{Amount of } NH_3 \text{ (mmol)}}{\text{Area of anode } (cm^2) \times \text{time (h)}} \times 100\%$$

Integration of PET hydrolysate oxidation and nitrate wastewater reduction

The alkali-assistant PET depolymerization method was utilized to depolymerize PET bottles into their constituent monomers.[1] Typically, 100 g of cleaned PET plastics were hydrolyzed into EG and TPA in an 1.5 M KOH solution at 180 °C for 12 h. The resulting hydrolysate was collected and directly used as anodic electrolyte. An enriched industrial wastewater containing 0.1 M NO_3^- concentration was constructed according to the previous reports.[2] A simulated wastewater was prepared, and KOH was subsequently added as electrolyte before being introduced into the cathodic chamber. PET hydrolysate oxidation coupled with nitrate wastewater reduction was performed on a membrane-electrode assembly (MEA) electrolyzer, using Ov-Co_3O_4/NF and Cu-$Ni(OH)_2$/NF as cathode and anode, respectively. The flow rate was controlled by a peristaltic pump, with flow rates of 1.2 and 2 mL min^{-1} for the cathode and anode, respectively.

Materials characterizations

The morphologies of samples were characterized by scanning electron microscopy (SEM, Hitachi Regulus8100) and transmission electron microscopy (TEM, Hitachi HT-7700). High-resolution TEM (HRTEM) and scanning TEM (STEM) were performed using uncorrected FEI Titan with Schottky field emission S-FEG source operated at 300 kV. Electron energy-

loss spectroscopy (EELS) mapping was carried out with Quantum Gatan Imaging Filter (GIF) detector with an energy dispersion of 0.5 eV per channel. The crystal structure was recorded on a Rigaku/MiniFlex600 diffractometer using Cu Kα radiation (λ = 1.5406 Å). X-ray photoelectron spectroscopy (XPS) was conducted on a Thermo Scientific ESCALAB 250XI spectroscopy equipped with Al Kα (hv=1486.6 eV) as the excitation source, and all binding energies were calibrated by the standard energy of 284.6 eV for C 1s. Fourier-transform infrared spectroscopy (FTIR) was carried out on a FT-IR spectrometer equipped with attenuated total reflection model (Thermo Scientific Nicolet iS5). ^{1}H nuclear magnetic resonance (NMR) spectroscopy was performed on JNM-ECZ500R to collect the chemical shifts of products. Electron spin resonance (ESR) measurements were performed on a Bruker A300 spectrometer.

***In-situ* Raman**: A homemade Raman cell was used to perform *in-situ* Raman measurement, with Hg/HgO electrode as the reference electrode and graphite rod as counter electrode. An electrochemical workstation (Corrtest, CS300MA) was utilized to supply voltage during the experiment. Raman spectra were recorded using a Raman spectrometer (Renishaw) equipped with a 532 nm excitation laser light. Raman frequencies were calibrated using a Si wafer.

***In-situ* FTIR**: *In-situ* Fourier transform infrared (FTIR) spectroscopy was employed on an IRTracer-100 FTIR spectrometer equipped with mercury cadmium telluride (HgCdTe) detector. For the preparation of the working electrode, 5 mg O_V-Co_3O_4 power was dispersed in a mixture solution containing ethanol, DI water, and Nafion under ultrasonic conditions. The resulting ink was deposited onto a self-prepared Au film, which was fabricated by chemically reducing commercial gilding liquid on the surface of a silicon prism. The electrolyte for nitrate reduction consisted of NO_3^- (0.1 M), KOH (0.01 M), and K_2SO_4 (0.4 M). The spectra were collected at interval voltages after electrolysis for 5 min. Prior to each measurement, the background spectrum of the catalyst electrode was acquired at an open-circuit voltage for baseline calibration.

Product analysis

The liquid products from EGOR, such as FA and GA, were identified by high-performance liquid chromatography (HPLC, Waters2489) with Agilent SB-AQ column and UV-Vis

detector. A mobile phase consists of 10 mM NaH_2PO_4 solution and methanol with the volume ratio of 95 to 5. The flow rate of the resulting mobile phase was controlled at 0.8 mL min^{-1}.

The concentration of NH_3 in the catholyte was quantitatively determined using the indoxyl blue method. The chromogenic agent (solution A) was prepared by mixing NaOH solution (1 M), with salicylic acid (5 wt%), sodium citrate (5 wt%). The oxidation agent (solution B) consisted of NaClO (0.05 M) and NaOH (2 M). Sodium nitrosoferricyanide (0.1 g) was dissolved into 10 mL DI water to form solution C. Then, 1 mL of solution A, 0.5 mL of solution B, 0.1 mL of solution C were added to 2 mL of diluted electrolyte. After 30 minutes at room temperature, the absorbance at 655 nm was measured using ultraviolet-visible spectrophotometry. The concertation of NO_2^- was quantified by the Griess test. Typically, N-(1-naphthyl) ethylenediamine dihydrochloride (0.2 g), p-aminobenzenesulfonamide (4.0 g) and H_3PO_4 (10 mL) were dissolved into 50 mL of deionized water, serving as chromogenic agent. Then, 0.2 mL of resulting chromogenic agent was added to 2 mL of diluted electrolyte. After 20 minutes at room temperature, its absorbance at 540 nm was measured using ultraviolet-visible spectrophotometry. Finally, the concertation of NO_2^- was calculated based on the calibration curve.

Theoretical calculation

All theoretical calculations were performed using the Vienna ab initio simulation package (VASP) code based on the first-principles of density functional theory (DFT) framework.[3] The projector-augmented wave pseudopotentials were applied to describe the electron–ion interaction.[4] The electronic exchange-correlation interaction effect was evaluated through the generalized gradient approximation (GGA) with Perdew-Burke-Ernzerh (PBE) of exchange-correlation function and the van der Waals interactions were considered using the DFT-D4 method.[5, 6] The stoichiometric Co_3O_4 (311) surface and $Ni(OH)_2$ (001) facet were modeled with a thickness of 20 Å vacuum in the Z direction. A cutoff energy of 520 eV was employed for the plane wave basis to ensure convergence. All the structures were optimized with energy and force convergence criterions of 10^{-5} eV and 0.02 eV $Å^{-1}$, respectively. To account for strongly correlated interactions in transition metal oxides, additional Hubbard U term with U_{eff} values of 3.0 eV and 5.5 eV were applied for Co and Ni cations, respectively. The band center (ε) was determined by taking the centroid of the projected density of states relative to

the Fermi level. The projected crystal orbital Hamilton population (pCOHP) analysis was carried out using LOBSTER program.[7] The adsorption energy was calculated through the equation of E = E_(sub+mol) – E_sub – E_mol, where E_(sub+mol) is the total energy of the adsorbed system, E_sub is the energy of the optimized clean surface slabs and E_mol is the energy of adsorbed molecules. The Gibbs free energy change (ΔG) of each elementary step was calculated by $\Delta G = \Delta E + \Delta ZEP - T\Delta S$, where ΔE is the adsorption enthalpy difference, ΔZPE is the difference of zero-point energies, and ΔS is the change of entropy.

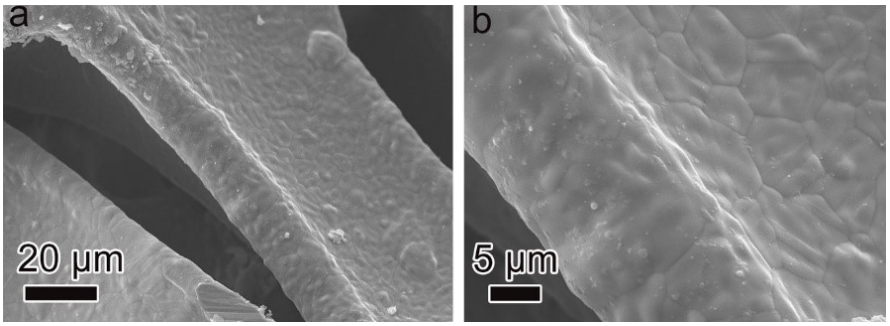

Fig. S1 (a, b) SEM images of bare NF.

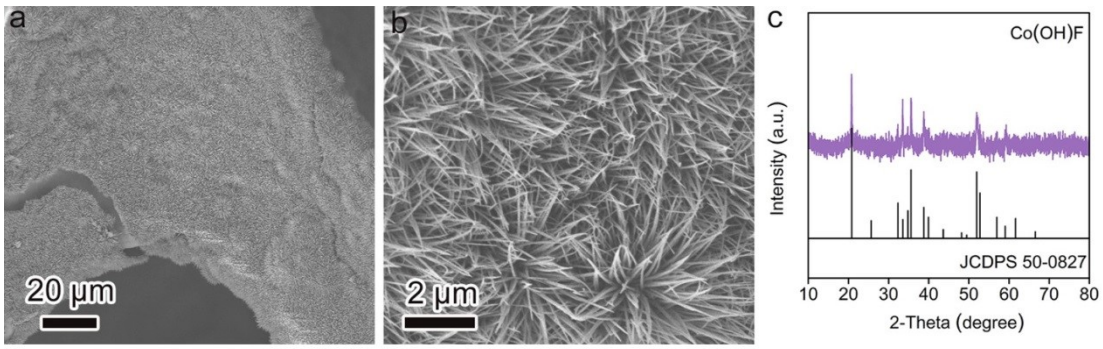

Fig. S2 (a,b) SEM images of Co(OH)F/NF and (c) XRD pattern of Co(OH)F powder scrapped from the NF substrate.

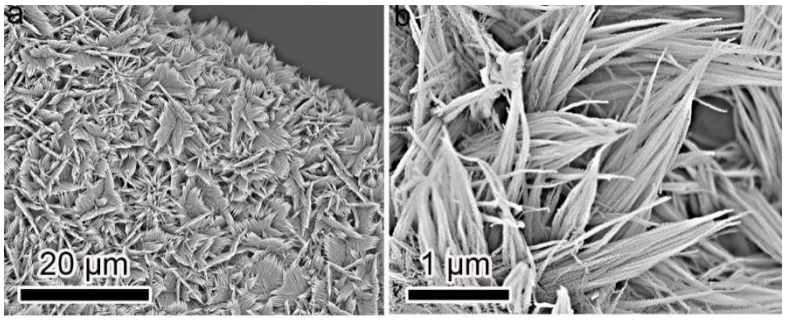

Fig. S3 SEM images of Co_3O_4/NF.

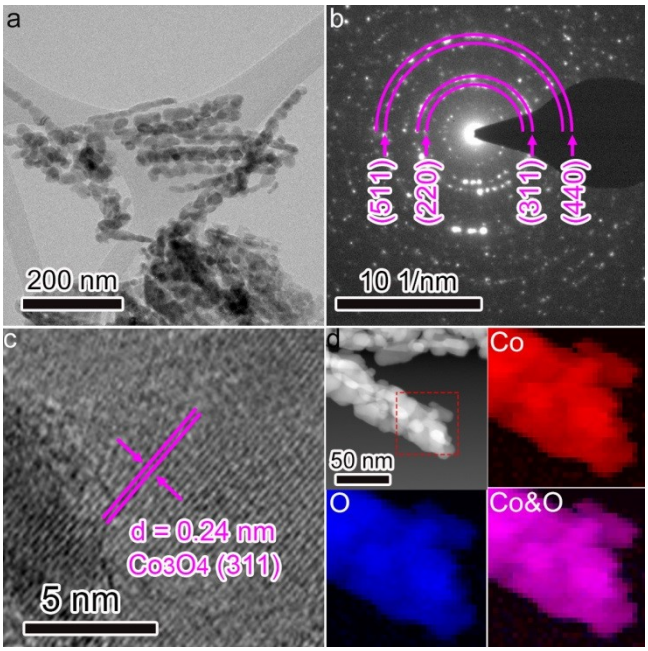

Fig. S4 (a) TEM image, (b) SAED pattern, (c) HRTEM image, (d) HAADF-STEM image and its corresponding EELS maps of Co_3O_4/NF.

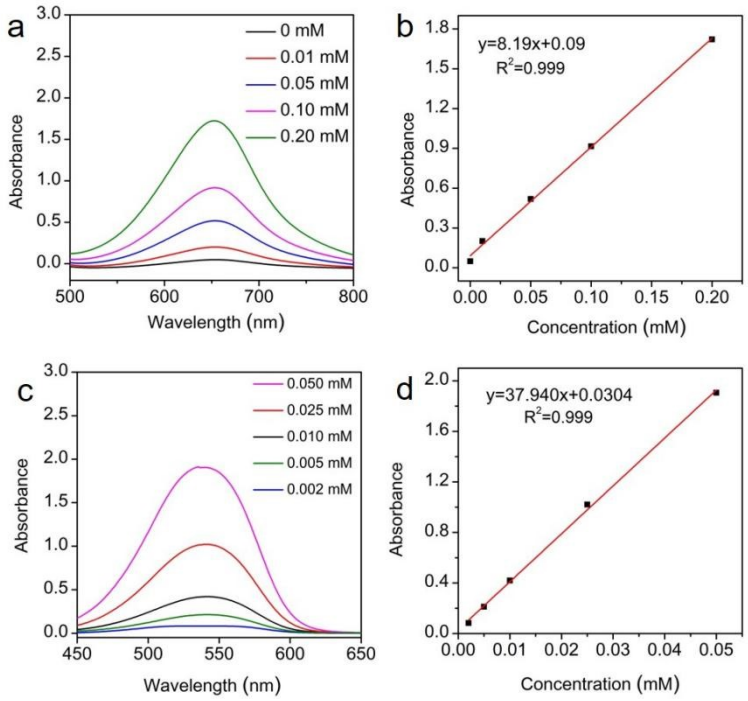

Fig. S5 (a) UV-vis absorption spectra of NH_4Cl and (b) the corresponding calibration curves; (c) UV-vis absorption spectra of $NaNO_2$ and (d) the corresponding calibration.

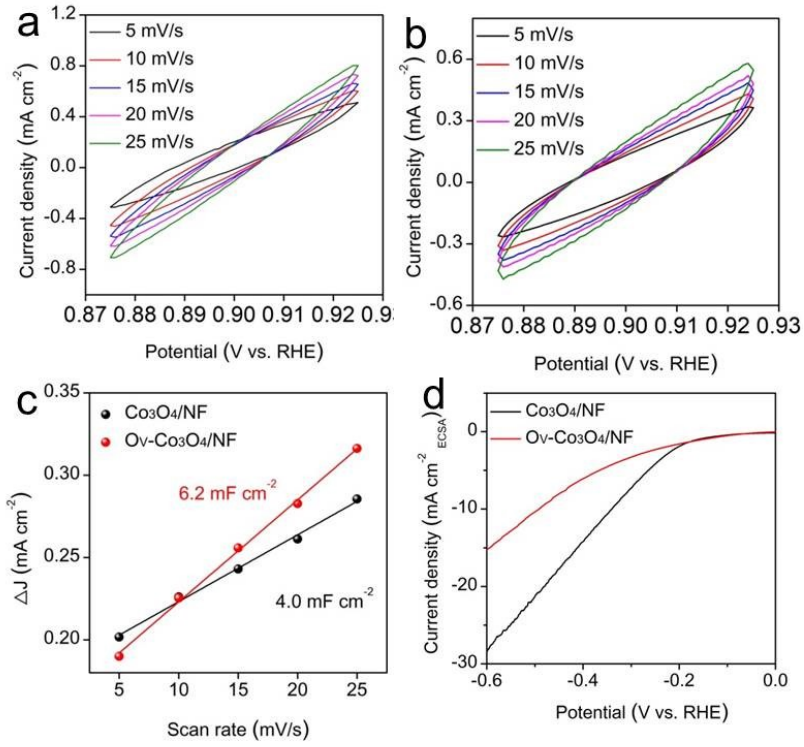

Fig. S6 (a, b) CV curves of Co_3O_4/NF and O_V-Co_3O_4/NF electrodes in the non-Faradaic capacitive range at the scan rate of 5~25 mV s^{-1}. (c) The plots of Δj recorded at 0.905 V vs. RHE as a function of the scan rate for Co_3O_4/NF and O_V-Co_3O_4/NF. (d) NO_3^-RR activity normalized by ECSAs.

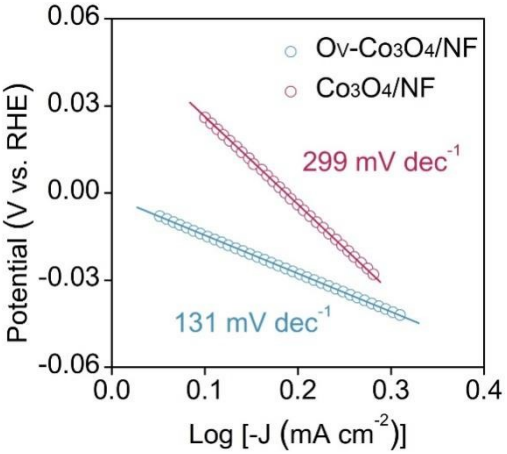

Fig. S7 Tafel slopes of Co_3O_4/NF and O_V-Co_3O_4/NF.

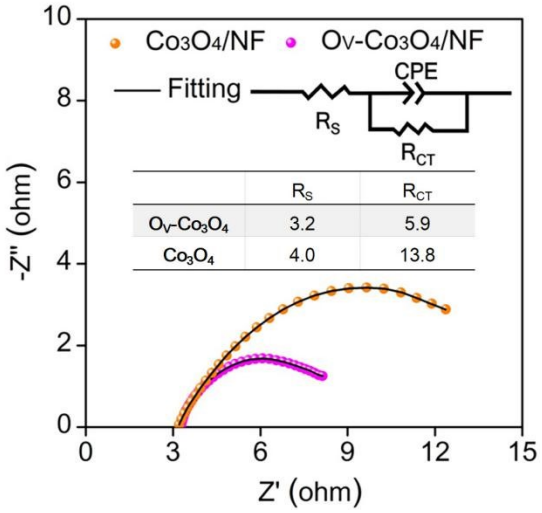

Fig. S8 EIS of Co_3O_4/NF and O_V-Co_3O_4/NF.

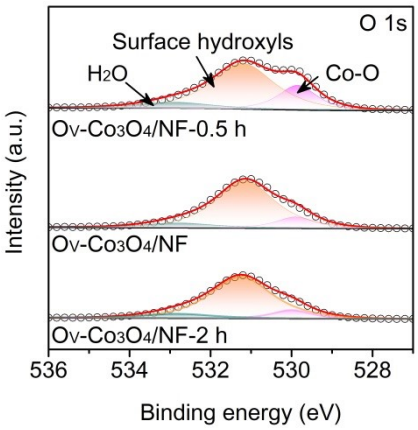

Fig. S9 O 1s XPS spectra of O_V-Co_3O_4/NF with various O_V concentrations prepared under different calcination times in H_2 atmosphere.

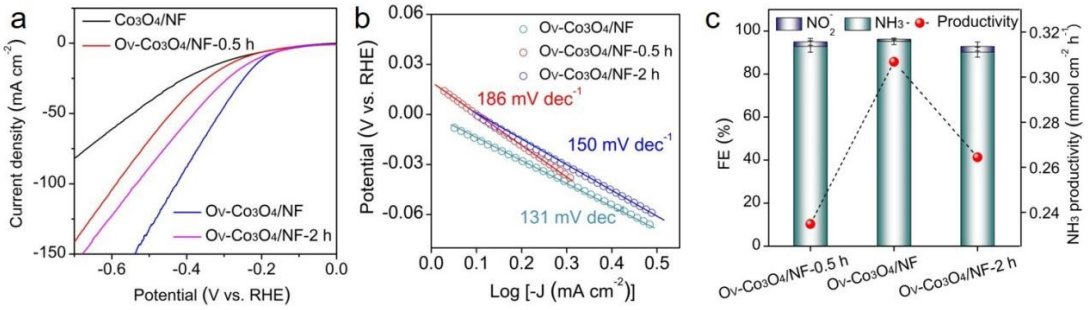

Fig. S10 (a) Polarization curves over O_V-Co_3O_4/NF catalysts with different O_V concentrations and (b) their corresponding Tafel plots, and (c) FE and productivity of NH_3 over O_V-Co_3O_4/NF catalysts with different O_V concentrations

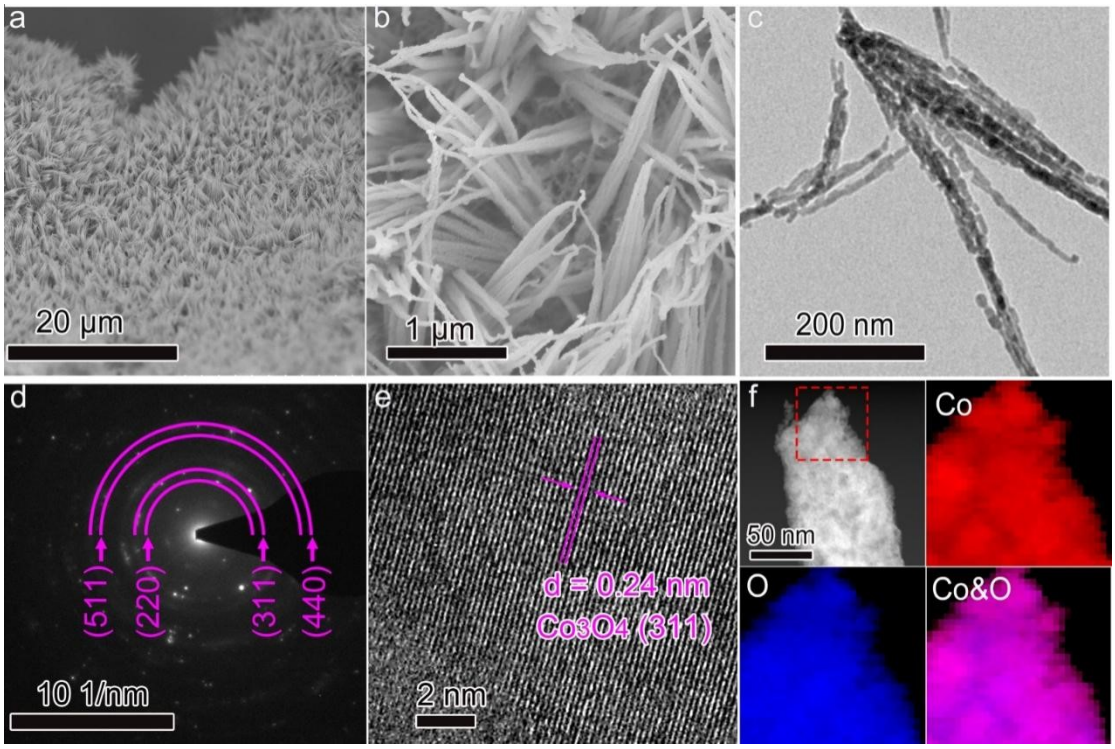

Fig. S11 (a,b) SEM images, (c) TEM images, (d) SAED pattern, (e) HRTEM image, (f) HAADF-STEM image and its corresponding EELS maps of the recovered O_V-Co_3O_4/NF catalyst.

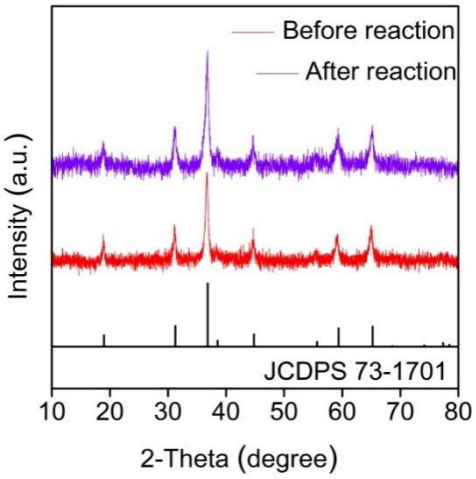

Fig. S12 XRD patterns of O_V-Co_3O_4/NF before and after NO_3^-RR.

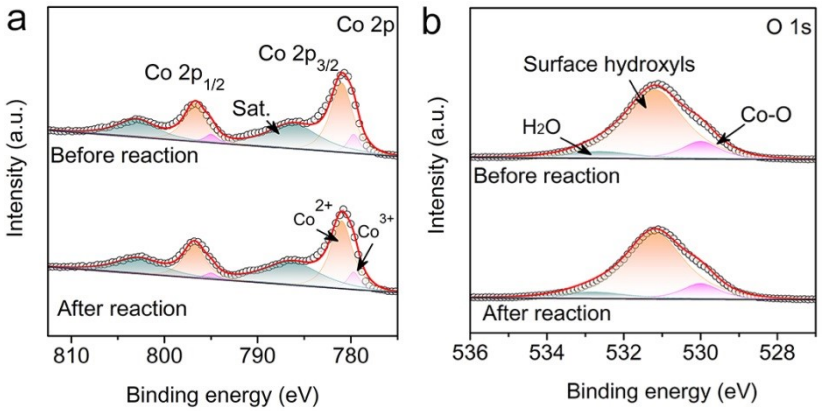

Fig. S13 (a) Co 2p and (b) O 1s XPS spectra of O_V-Co_3O_4/NF before and after reaction.

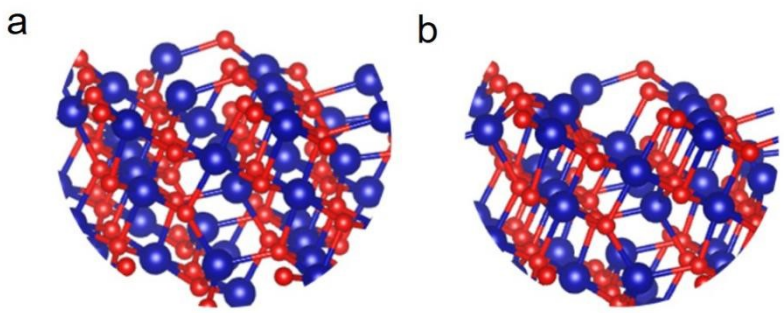

Fig. S14 The constructed model of the (311) plane of Co_3O_4 (a) and O_V-Co_3O_4 (b).

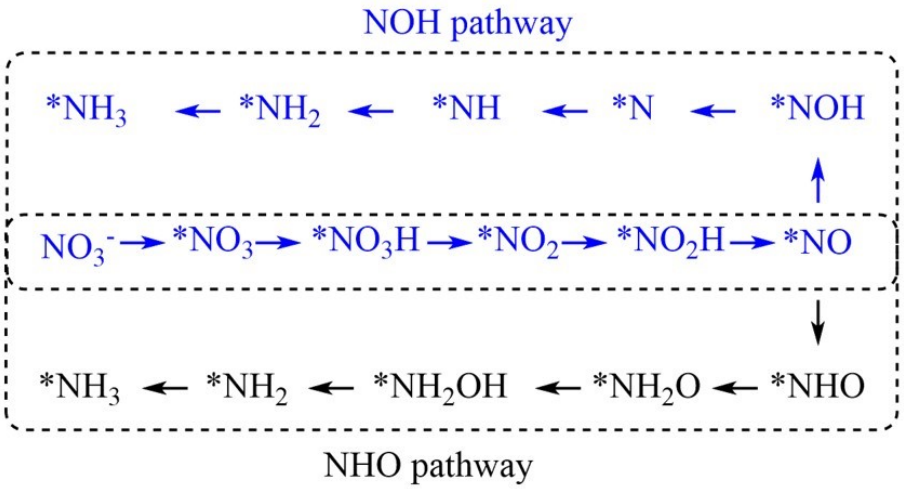

Fig. S15 Two typical pathways for NO_3^-RR.

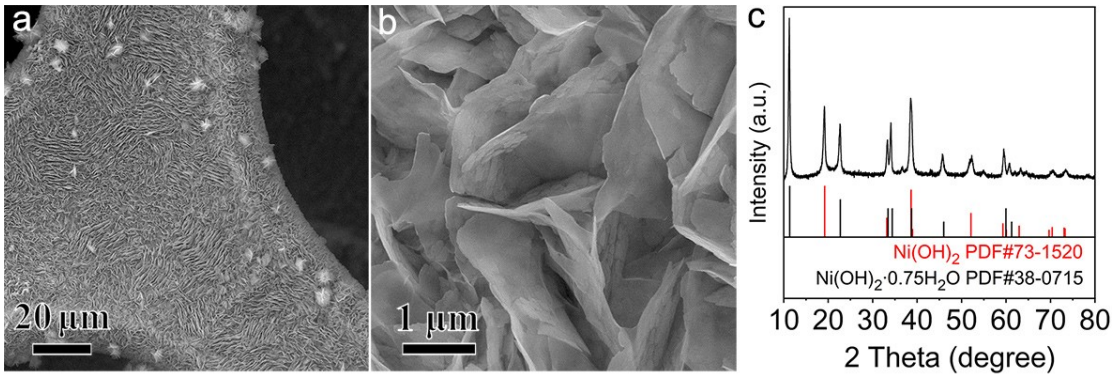

Fig. S16 (a,b) SEM images and (c) XRD pattern of Cu-Ni$(OH)_2 \cdot xH_2O$/NF.

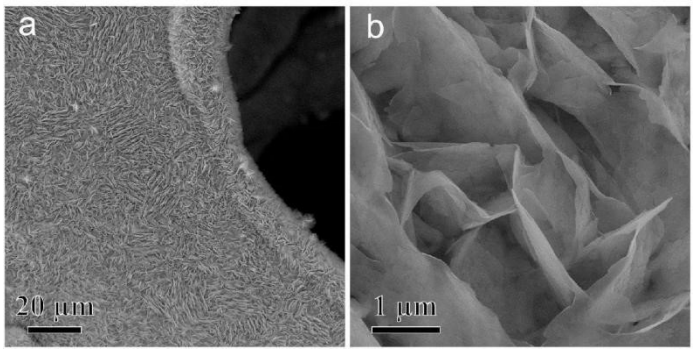

Fig. S17 (a,b) SEM images of $Ni(OH)_2$/NF.

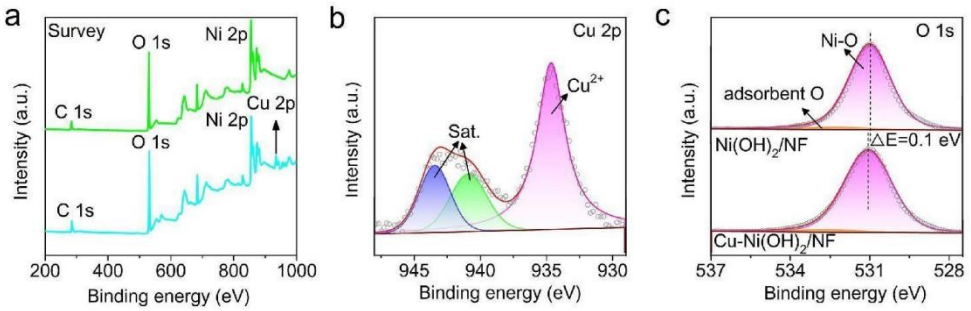

Fig. S18 (a) Survey XPS spectrum, and (b) Cu 2p and (c) O 1s high-resolution XPS spectra.

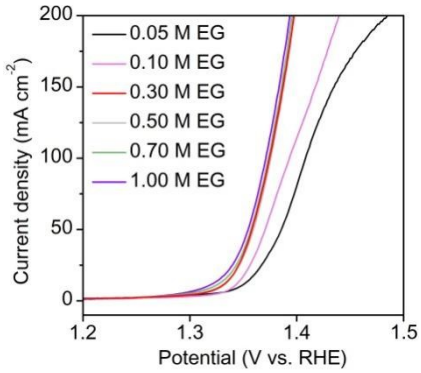

Fig. S19 LSV curves of Cu-Ni$(OH)_2$/NF in 1 M KOH solution with varying EG concentrations.

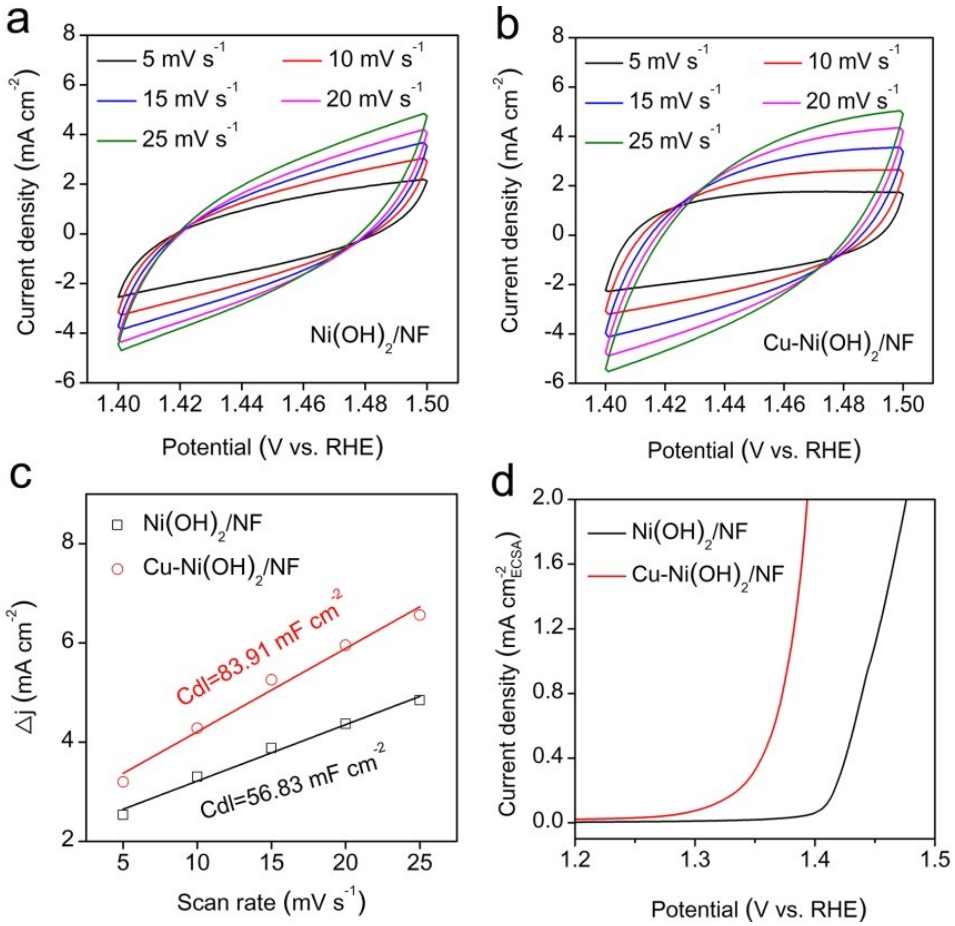

Fig. S20 CV curves of $Ni(OH)_2$/NF (a) and Cu-$Ni(OH)_2$/NF (b) in the non-Faradaic capacitive region at the scan rate of 5-25 mV s^{-1}. (c) The plots of Δj recorded at 1.45 V vs. RHE as a function of the scan rate for $Ni(OH)_2$/NF and Cu-$Ni(OH)_2$/NF. (d) The LSV curves of $Ni(OH)_2$/NF and Cu-$Ni(OH)_2$/NF normalized by their corresponding ECSA values.

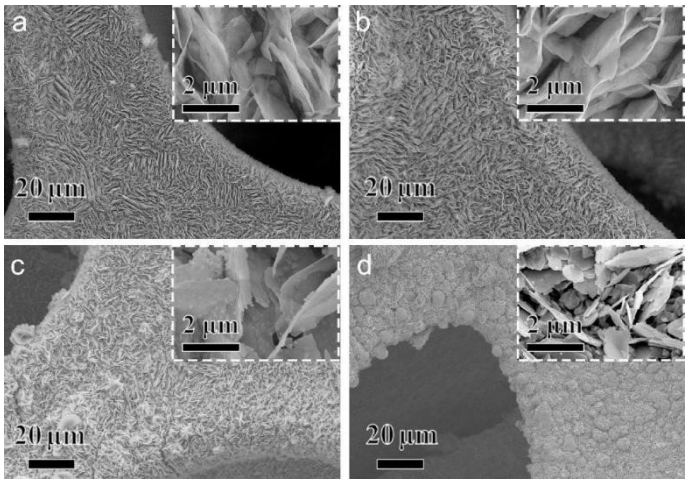

Fig. S21 SEM images Cu-Ni$(OH)_2$/NF with various molar ratios of Cu to Ni: (a) 1:19, (b) 1:9, (c) 1:5, and (d) 1:2.

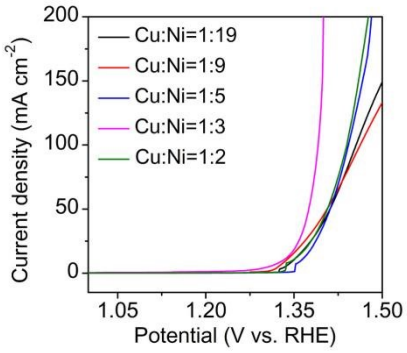

Fig. S22 LSV curves of Cu-Ni$(OH)_2$/NF with various molar ratios of Cu to Ni in 1 M KOH solutions.

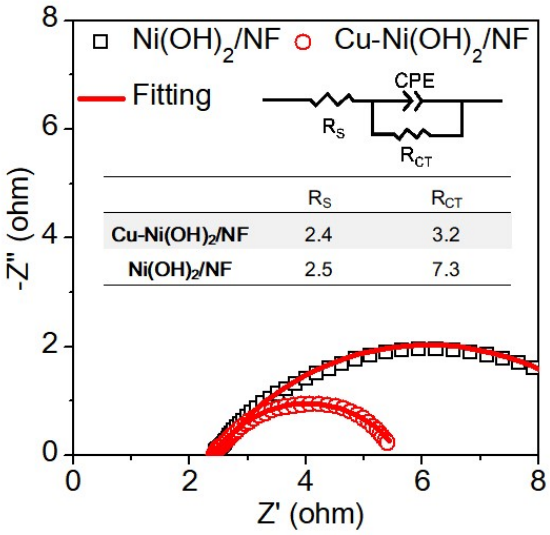

	R_S	R_{CT}
Cu-Ni(OH)$_2$/NF	2.4	3.2
Ni(OH)$_2$/NF	2.5	7.3

Fig. S23 Nyquist plots of Ni(OH)$_2$/NF and Cu-Ni(OH)$_2$/NF in 1 M KOH and 0.3 M EG.

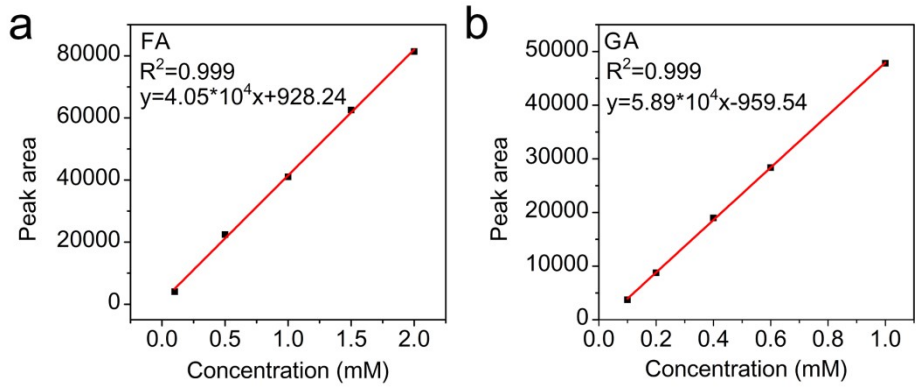

Fig. S24 The calibration curves of formic acid (FA) and glycolic acid (GA).

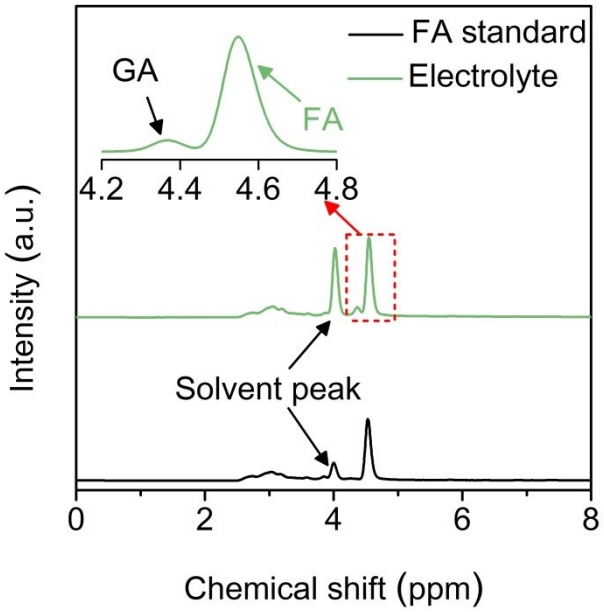

Fig. S25 HPLC spectra of post-reaction electrolyte.

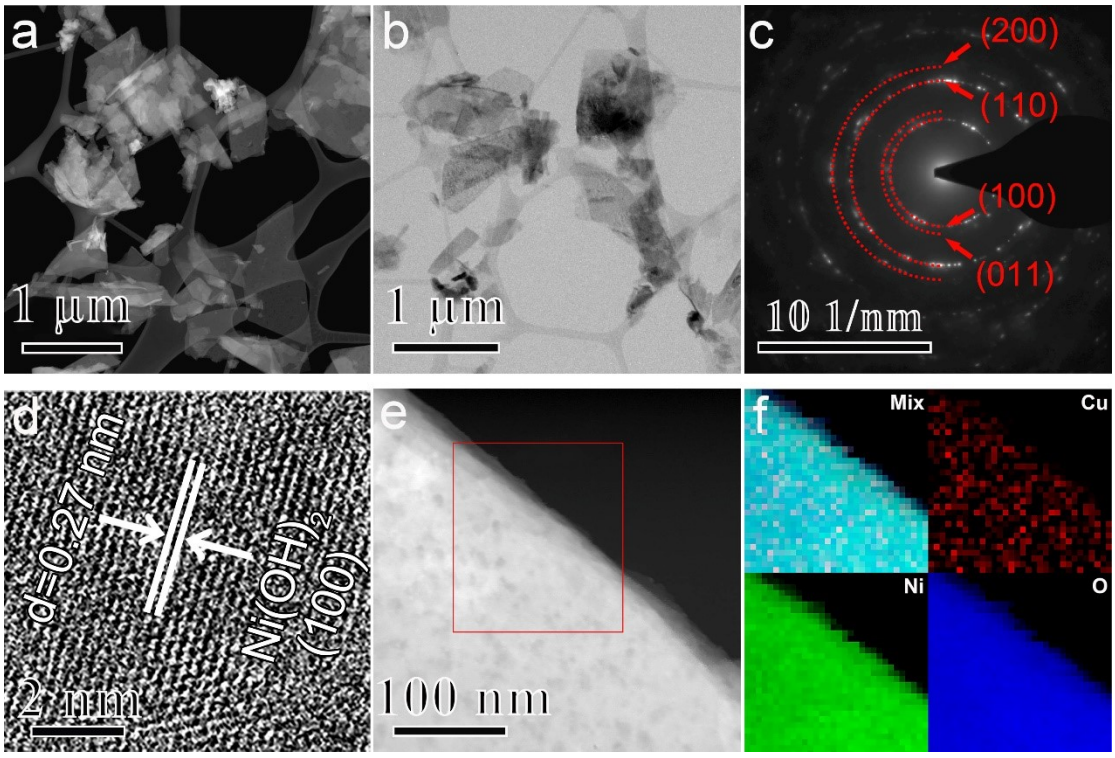

Fig. S26 Morphology characterizations of the recovered Cu-$Ni(OH)_2$/NF catalyst: (a) STEM image, (b) TEM image, (c) SAED patterns, (d) HRTEM image, (e) HAADF-STEM image, and (f) EELS mapping.

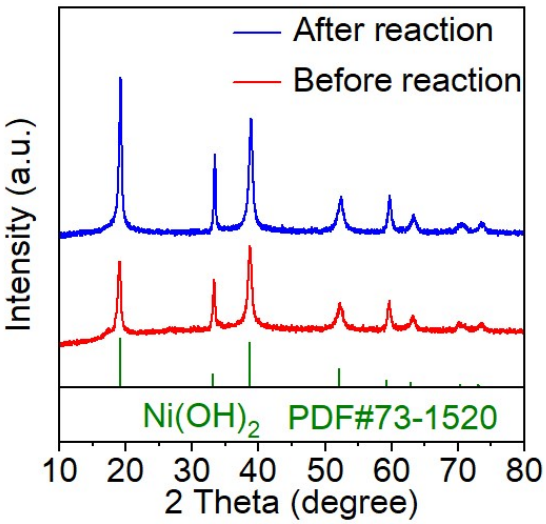

Fig. S27 XRD patterns of Cu-$Ni(OH)_2$ powders scrapped from the NF substrate before and after reaction.

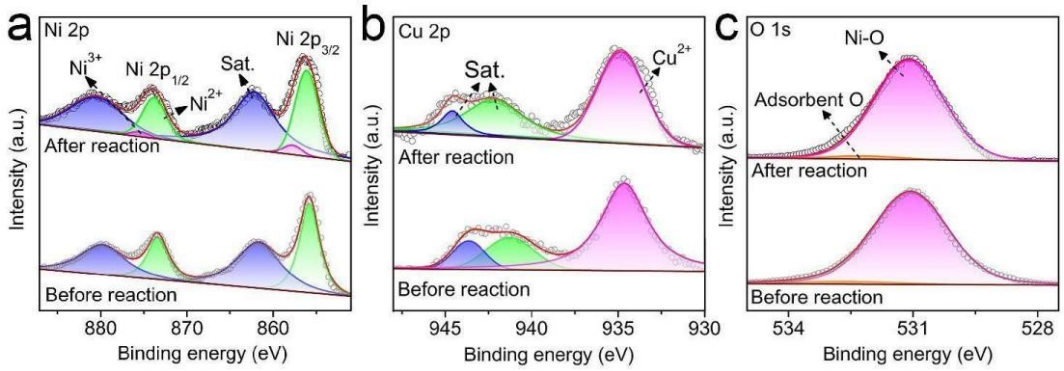

Fig. S28 XPS spectra of Cu-Ni$(OH)_2$/NF before and after reaction: (a) Ni 2p, (b) Cu 2p and (c) O 1s.

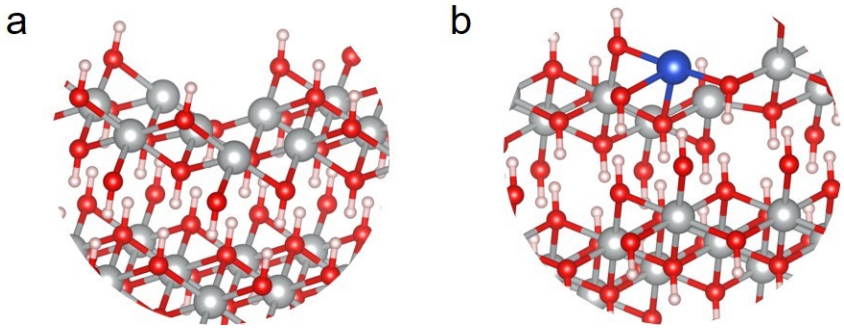

Fig. S29 The theoretical models of (a) $Ni(OH)_2$ (001) and (b) Cu-$Ni(OH)_2$ (001).

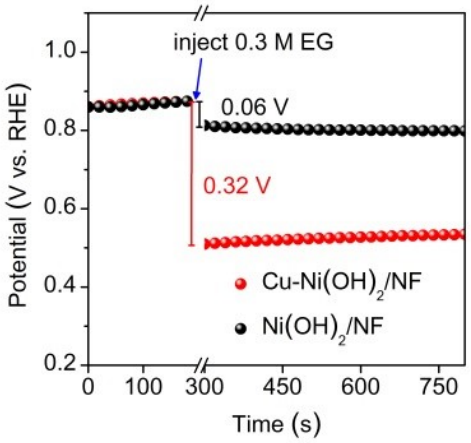

Fig. S30 The open-circuit potential (OCP) measurements of the Cu-$Ni(OH)_2$/NF and $Ni(OH)_2$/NF catalysts in 1 M KOH solution before and after EG introduction.

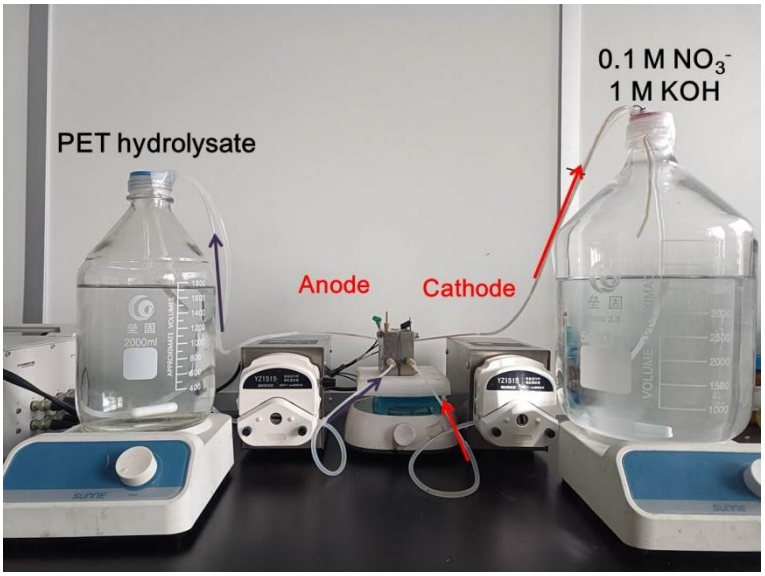

Fig. S31 The photograph of the MEA closed-loop flow reactor for PET hydrolysate oxidation coupled with simulated nitrate wastewater reduction. Note that the as-prepared O_V-Co_3O_4/NF and Cu-$Ni(OH)_2$/NF are utilized as cathode and anode, respectively. The flow rates of electrolyte are 1.2 and 2 mL min^{-1} in the cathode and anode, respectively.

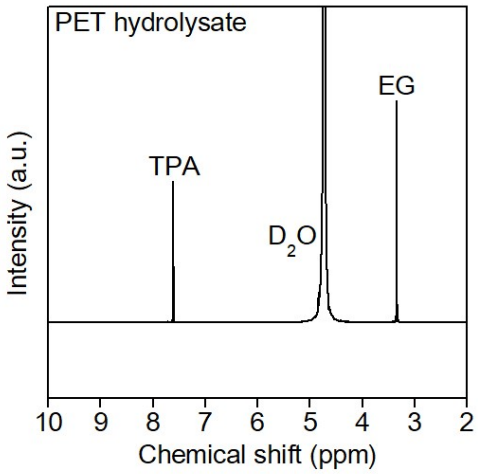

Fig. S32 ^{1}H NMR of PET hydrolysate.

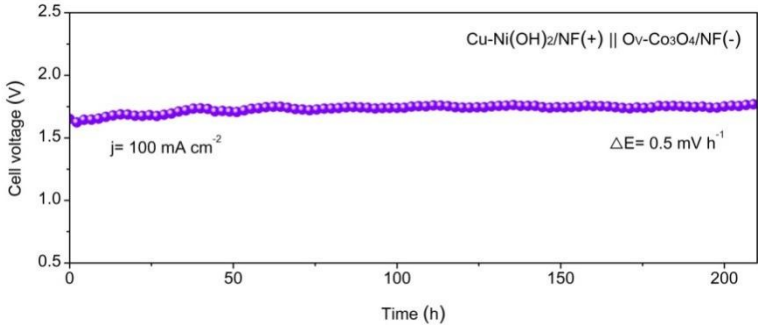

Fig. S33 Chronopotentiometry curves of Cu-Ni$(OH)_2$/NF(+)‖O_V-Co_3O_4/NF(-) for anodic PET hydrolysate oxidation and cathodic nitrate reduction at the current density of 100 mA cm^{-2}.

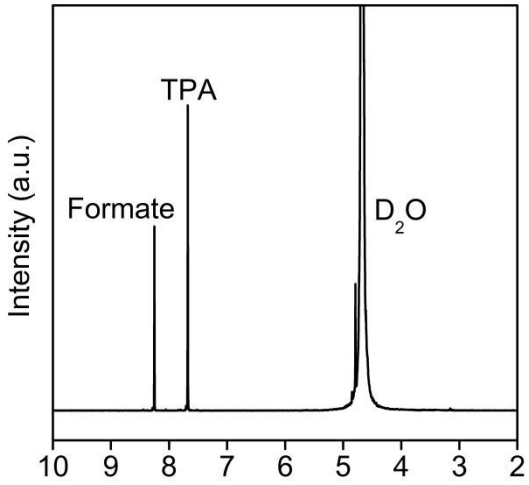

Fig. S34 ^{1}H NMR of the post-reaction electrolyte.

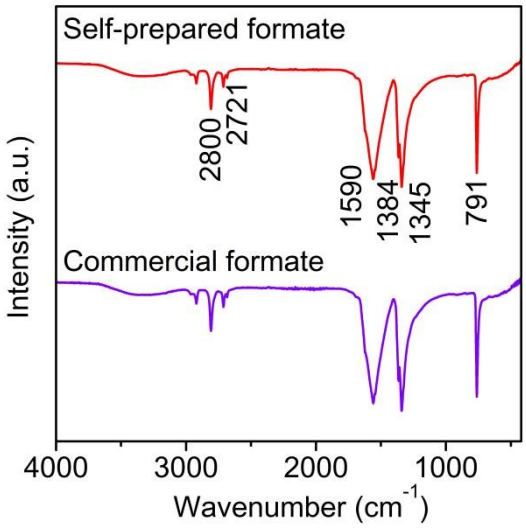

Fig. S35 FTIR spectra of the self-prepared formate and the standard sample.

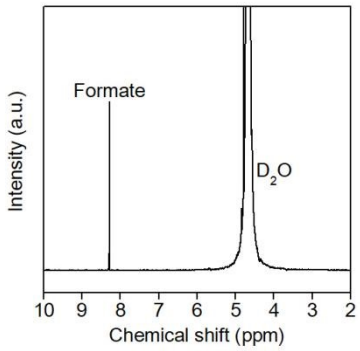

Fig. S36 ^{1}H NMR spectrum of self-prepared formate.

Table S1. Comparison of NO_3^-RR activity over O_V-Co_3O_4 with other reported catalysts.

Catalysts	Electrolyte	FE (%)	Ref.
O_V-Co_3O_4/NF	1.0 M KOH + 0.1 M KNO_3	95.2	This work
Cu_2O+Co_3O_4	0.1 M NaOH + 0.1 M $NaNO_3$	85.4	[8]
Fe/Ni_2P	0.2 M K_2SO_4 + 0.05 M KNO_3	94.3	[9]
Co-Fe@Fe_2O_3	0.5 M Na_2SO_4 + 0.05 M $NaNO_3$	85.2	[10]
Ni_3 N/N-C-800	0.5 M Na_2SO_4 + 0.2 M $NaNO_3$	85.0	[11]
CuCoSP	0.1M KOH + 0.01 M KNO_3	92.8	[12]
CuFe-450	1.0 M KOH + 0.1 M KNO_3	90.6	[13]
R-NiCu-OH	1.0 M KOH + 0.1 M KNO_3	72.0	[14]
CoP-CNS	1.0 M KOH + 1.0 M KNO_3	93.3	[15]
PdCuRu MSs	0.1 M KOH + 0.01 M KNO_3	95.0	[16]
$Pt_{0.9}$/$Ce_{0.5}$-SS	0.5 M Na_2SO_4 + 0.1 M KNO_3	94.1	[17]
Cu nanosheets	1.0 M KOH + 0.2 M KNO_3	95.0	[18]
Fe_2TiO_5	PBS + 0.1 M $NaNO_3$	90.1	[19]

Table S2. Comparison of EGOR activity over Cu-$Ni(OH)_2$/NF with other catalysts.

Catalysts	Electrolyte	FE (%)	Ref.
Cu-$Ni(OH)_2$/NF	0.3 M EG+1 M KOH	98.1	This work
CoFe-P/NF	0.05 M EG+1 M KOH	90.0	[20]
B,Co-NiS	0.1 M EG+1 M KOH	95.7	[21]
Au/$Ni(OH)_2$	1 M EG+1 M KOH	96.5	[22]
NiCu/NF	0.3 M EG+1 M KOH	91.8	[23]
Ni-MOF@MnCo-OH	0.1 M EG+1 M KOH	90.7	[24]
$CuCo_2O_4$/NF	0.5 M EG+5M KOH	93.0	[25]
Ni_3N/W_5N_4	0.1 M EG+1 M KOH	85.0	[26]
Ru-CoOOH	0.1 M EG+1 M KOH	96.5	[27]
$NiCo_2O_4$/CFP	0.1 M EG+1 M KOH	93.2	[28]
OMS-Ni_1-CoP	0.5 M EG+1 M KOH	96.0	[29]
Pd-NiTe/NF	0.5 M EG+1 M KOH	96.5	[30]
$CoNi_{0.25}P$/NF	0.3 M EG+1 M KOH	91.7	[31]

Table S3. The price of commercial chemicals

Chemicals	Price ($ ton^{-1})	Ref.
PET wastes	390	[31]
KOH	850	[32]
H_2O	0.22	[33]
TPA	1260	[34]
HCl	21.5	[32]
Formate	650	[35]
NH_4Cl	531	[36]

Supplementary Note 1

To evaluate the process of PET upgrading coupled with nitrate reduction in industry, a well-accepted economical model was adopted.[37-39] Typically, several operational parameters such as the electrolyzer and operational cost should be specified prior to the economic analysis. Initially, the daily operational capacity for waste PET plastic was set at 200 tons, which aligns with previous literature.[31] During electrocatalysis, an electrolyzer is necessary for PET upgrading, and its price is fixed at \$677 per m^2.[40] The electricity price used in the system is set at \$ 0.03 kWh^{-1}.[41, 42] The cost of the facility for plastic treatment, including set-up for PET hydrolysis, separation, and filtration, is assumed to be 30% of electricity cost. In addition, the operational cost accounts for 10% of the total equipment cost, based on hypothesis from previous literature.[1] Considering additives present in plastic, the proportion of efficient consistent monomers (TPA and EG) in waste PET is 85%.

In the experimental section focused on the study of EG oxidation paired with NO_3^- reduction reaction, the Faradaic efficiency for formate generation at the anode was recorded at 98.23%, while FE for NH_3 production at the cathode was 95%. The operational voltage was set at 1.7 V, with an applied current density of 100 mA cm^{-2}. For comparison, when EG oxidation is paired with OER, the Faradaic efficiency for O_2 is 100%. This operation is conducted at 2.2 V versus RHE, with a current density of 100 mA cm^{-2}.

Typically, the collected PET wastes firstly undergo a series of process staring with cleaning, and hydrolysis, followed by electrolysis step using the obtained hydrolysate as feedstock. Subsequently, TPA precipitate is extracted from anode electrolyte by adding formic acid until the pH of solution to neutral conditions, and then the solvent in filtrate is evaporated to yield formate product. Simultaneously, ammonia dissolved in the cathode electrolyte can be separated through evaporation and subsequently neutralized by an HCl solution.

1. Pretreatment set-up cost

According to the procedure, the equipment required for PET hydrolysis is essential. The annual cost for alkali-assisted PET depolymerization is assumed to be $\$10\times 10^6$ per year.

2. Investment for electrolyzer

$$I = \frac{Q}{Time\ in\ one\ day \times capacity\ factor}$$

Where Q is the total charge; capacity factor is 0.8.

$$Q = \frac{Mass\ of\ EG \times F \times N}{Molar\ mass\ of\ EG \times Faradaic\ efficiency} = \frac{200 \times 0.85 \times 10^6 \times 96485 \times 6}{192 \times 0.9823} = 5.22 \times 10^{11}\ C$$

Where F is the Faraday's constant (96485 C mol^{-1}); N is the electron transfer from EG to FA (N=6); Faradaic efficiency is 98.23%.

$$I = \frac{Q}{Time\ in\ one\ day * \ capacity\ factor} = \frac{5.22 \times 10^{11}}{24 \times 3600 \times 0.8} = 7.55 \times 10^6\ A$$

Area of electrolyzer = $\frac{I}{i}$ (m^2) = $7.55 \times 10^3\ m^2$

Where *I* is the total consumed electric current; *i* is the current density (100 mA cm^{-2}). Therefore, the cost for electrolyzer facility is followed

Cost of electrolyzer = Area× 677 per m^{-2} = 5.11×10^6 $

Noting that lifetime of the electrolyzer should be considered. Herein, we assume that the electrolyzer has a 10-year lifetime.

$$Cost\ of\ electrolyser = \frac{5.11 \times 10^5}{365} = 1400\ \$/d$$

3. Electricity for PET upgrading

The consumed electricity during electrochemical upgrading

$$P = U \times I \times t = 1.7\ V \times 7.55 \times 10^6\ A \times 19.2\ h\ = 2.46 \times 10^5\ kWh$$

The price of electricity was estimated to be 0.03 $ kWh^{-1}

The price of electricity= $2.46 \times 10^5 \times$ 0.03 $ kWh^{-1} = 7380 $/d

4. The separation costs are expected to be 30% of total electricity costs.

$$Cost\ of\ separation = The\ electricity\ cost \times 30\% = 2214\ \$/d$$

5. Operation cost is assumed to be 10% of the capital costs and is calculated as:

$$Cost\ of\ operation\ cost = Cost\ of\ capital\ investment \times 10\% = 2879.5\ \$/d$$

6. Materials cost

Based on the experimental procedure outlined above, chemicals such as PET waste,

KOH, water, and formic acid were utilized during the electrocatalysis. After calculation, the EGOR process requires 200 tons of PET, 165.2 tons of KOH, and 2950 tons of water. Additionally, 54.74 tons of formic acid is used to precipitate TPA and neutralize any residual alkali. For the NO_3^-RR process in the cathode, 371.7 tons of KOH and 6640 tons of water are needed. Furthermore, 24.2 tons of hydrochloric acid is employed to absorb the ammonia.

$$Materials\ costs = mass\ of\ PET\ waste \times cost\ of\ PET + mass\ of\ KOH \times cost\ of\ KOH + mass\ of\ formic\ acid \times cost\ of\ formic\ acid + mass\ of\ HCl \times cost\ of\ HCl + mass\ of\ H_2O \times cost\ of\ H_2O = 242946.1\ \$/d$$

In summary, the total input for EGOR integrated with NO_3^-RR

$$Total\ cost = Pretreatment\ equipment\ cost + Electrolyzer\ cost + Opera + Seperation\ cost + Materials\ cost = 27395 + 1400 + 2879.5 + 7380 + 2214 + 242946.1 = 284214.6\ \$/d$$

7. Output chemicals

The total price of products generated during this system, including TPA, formate, and NH_4Cl, has been calculated. This process yields 146 tons of TPA, 247.8 tons of formate, and 35.5 tons of NH_4Cl. Therefore, the product value can be calculated as:

$$Total\ price\ of\ output\ chemicals = Mass\ of\ TPA_{\times}\ Cost\ of\ TPA + Mass\ of\ formate_{\times}\ Cost\ of\ formate + Mass\ of\ NH_4Cl_{\times}\ Cost\ of\ NH_4Cl = 146_{\times}\ 1260 + 247.8_{\times}\ 650 + 35.5_{\times}\ 531 = 363880.5\ \$/d$$

Therefore, the profit is estimated as follows:

$$Profit = Output\ values - input\ costs = 363880.5 - 284214.6 = 79665.9\ \$/d$$

TEA for NO_3^-RR coupled with OER

Given that the anode reaction is the oxygen evolution reaction, the setup investment for plastic depolymerization can be ignored. In another case, the separation cost for products can also be reduced because oxygen can be easily removed from the electrolyte. Therefore, the separation costs are reduced to 10% of the electricity costs.

1. Electrolyzer costs

Similar to the NO_3^-RR coupled with EGOR system, an electrolyzer is also required to reduce NO_3^- into NH_3 and oxidize water into oxygen. For comparison, the same operational current density (100 mA cm^{-2}) is used for this system. Therefore, the fixed investment is calculated.

$$Cost\ of\ electrolyser = \frac{5.11\times10^5}{365} = 1400\ \$/d$$

2. Electricity costs

Based on the results in linear sweep voltage curve, the potential of 2.2 V can driver NO_3^- RR coupled with OER to reach designed current density.

The electricity price was estimated

$$P = U\times I\times t = 2.2\ V \times 7.55\times10^6\ A\times19.2\ h = 3.19\times10^5\ kWh$$

The price of electricity was estimated to be 0.03 \$ kWh^{-1}

The price of electricity= $3.19\times10^5\times$ 0.03 \$ kWh^{-1}= 9570 \$/d

3. Separation cost

$$Cost\ of\ separation = The\ electricity\ cost\times 10\% = 957\ \$/d$$

4. The operation cost is 10% of capital cost.

$$Cost\ of\ operation = The\ electrolyzer\ cost\times 10\% = 140\ \$/d$$

5. Input chemicals

NO_3^-RR requires 6640 tons of H_2O and 371.7 tons of KOH. OER requires 6640 tons of H_2O and 371.7 tons of KOH. Since potassium hydroxide can be reused, its usage can be averaged on a daily basis. 24.2 tons of hydrochloric acid is required to absorb the ammonia.

$$Cost\ of\ water = Mass\ of\ H_2O\times Cost\ of\ H_2O = 6640\times 0.22 = 1460.8\ \$/d$$

$$Cost\ of\ HCl = Mass\ of\ HCl\times Cost\ of\ HCl = 24.2\times21.5 = 520.3\ \$/d$$

$$\begin{aligned} &Total\ input\ cost \\ &= Electrolyzer\ cost + Operating\ cost + Electricity\ cost + S \\ &+ Materials\ cost \\ &= 1400 + 140 + 9570 + 957 + 1981.1 = 14048.1\ \$/d \end{aligned}$$

6. Products value

NH_4Cl and oxygen is the product in cathode and anode, respectively. After calculation, 35.5 tons of NH_4Cl and 10.6 tons of oxygen are gained.

$$\begin{aligned} &Total\ price\ of\ output\ chemicals \\ &= Mass\ of\ oxygen\times Cost\ of\ oxygen + Mass\ of\ NH_4Cl\times Cost\ of\ NH_4Cl \\ &= 10.6\times 35 + 35.5\times 531 = 19221.5\ \$/d \end{aligned}$$

$$Profit = Output\ values - input\ costs = 19221.5 - 14048.1 = 5173.4\ \$/d$$

References

1. M. Du, Y. Zhang, S. Kang, C. Xu, Y. Ma, L. Cai, Y. Zhu, Y. Chai and B. Qiu, *Small*, 2023, **19**, 2303693.
2. Y. Chen, P. Ammari-Azar, H. Liu, J. Lee, Y. Xi, M. J. Castellano, S. Gu and W. Li, *EES Catal.*, 2023, **1**, 504-515.
3. G. Kresse and J. Furthmüller, *Comp. Mater. Sci.*, 1996, **6**, 15-50.
4. P. E. Blöchl, *Phys. Rev. B*, 1994, **50**, 17953.
5. J. P. Perdew, K. Burke and M. Ernzerhof, *Phys. Rev. Lett.*, 1996, **77**, 3865.
6. E. Caldeweyher, C. Bannwarth and S. Grimme, *J. Chem. Phys.*, 2017, **147**.
7. R. Nelson, C. Ertural, J. George, V. L. Deringer, G. Hautier and R. Dronskowski, *J. Comp. Chem.*, 2020, **41**, 1931-1940.
8. J. Zhang, W. He, T. Quast, J. R. Junqueira, S. Saddeler, S. Schulz and W. Schuhmann, *Angew. Chem.Int. Ed.*, 2023, **62**, e202214830.
9. R. Zhang, Y. Guo, S. Zhang, D. Chen, Y. Zhao, Z. Huang, L. Ma, P. Li, Q. Yang and G. Liang, *Adv. Energy Mater.*, 2022, **12**, 2103872.
10. S. Zhang, M. Li, J. Li, Q. Song and X. Liu, *Proc. Natl Acad. Sci.*, 2022, **119**, e2115504119.
11. X. Zhang, G. Ma, L. Shui, G. Zhou and X. Wang, *Chem. Eng. J.*, 2022, **430**, 132666.
12. W. He, J. Zhang, S. Dieckhöfer, S. Varhade, A. C. Brix, A. Lielpetere, S. Seisel, J. R. Junqueira and W. Schuhmann, *Nat. Commun.*, 2022, **13**, 1129.
13. R. Hao, L. Tian, C. Wang, L. Wang, Y. Liu, G. Wang, W. Li and G. A. Ozin, *Chem Catal.*, 2022, **2**, 622-638.
14. S. Li, P. Ma, C. Gao, L. Liu, X. Wang, M. Shakouri, R. Chernikov, K. Wang, D. Liu, R. Ma and J. Wang, *Energy Environ. Sci.*, 2022, **15**, 3004-3014.
15. K. Fan, W. Xie, J. Li, Y. Sun, P. Xu, Y. Tang, Z. Li and M. Shao, *Nat. Commun.*, 2022, **13**, 7958.
16. L. Sun, H. Yao, F. Jia, Y. Wang and B. Liu, *Adv. Energy Mater.*, 2023, **13**, 2302274.
17. D. Chen, S. Zhang, D. Yin, W. Li, X. Bu, Q. Quan, Z. Lai, W. Wang, Y. Meng and C. Liu, *Adv. Energy Mater.*, 2023, **13**, 2203201.
18. Y. Fu, S. Wang, Y. Wang, P. Wei, J. Shao, T. Liu, G. Wang and X. Bao, *Angew. Chem. Int. Ed.*, 2023, **62**, e202303327.
19. H. Du, H. Guo, K. Wang, X. Du, B. A. Beshiwork, S. Sun, Y. Luo, Q. Liu, T. Li and X. Sun, *Angew. Chem.*, 2023, **135**, e202215782.
20. J. Chang, L. Wang, D. Wu, F. Xu, K. Jiang, Y. Guo and Z. Gao, *J. Coll. Interf. Sci.*, 2024, **655**, 555-564.
21. Z. Chen, W. Wei, Y. Shen and B.-J. Ni, *Green Chem.*, 2023, **25**, 5979-5988.
22. D. Du, F. Kang, S. Yang, B. Shao and J. Luo, *Sci. China Chem.*, 2024, **67**, 1539-1544.
23. H. Kang, D. He, X. Yan, B. Dao, N. B. Williams, G. I. Elliott, D. Streater, J. Nyakuchena, J. Huang and X. Pan, *ACS Catal.*, 2024, **14**, 5314-5325.
24. W. Li, D. Xiao, X. Gong, X. Xu, F. Ma, Z. Wang, P. Wang, Y. Liu, Y. Dai and Z. Zheng, *Chem.l Eng. J.*, 2024, **480**, 148087.
25. F. Liu, X. Gao, R. Shi, E. C. M. Tse and Y. Chen, *Green Chem.*, 2022, **24**, 6571-6577.
26. F. Ma, S. Wang, X. Gong, X. Liu, Z. Wang, P. Wang, Y. Liu, H. Cheng, Y. Dai and Z. Zheng, *Appl. Catal. B: Environ. Energy*, 2022, **307**, 121198.

27. T. Ren, Z. Yu, H. Yu, K. Deng, Z. Wang, X. Li, H. Wang, L. Wang and Y. Xu, *ACS Nano*, 2023, **17**, 12422-12432.
28. J. Wang, X. Li, M. Wang, T. Zhang, X. Chai, J. Lu, T. Wang, Y. Zhao and D. Ma, *ACS Catal.*, 2022, **12**, 6722-6728.
29. N. Wang, X. Li, M.-K. Hu, W. Wei, S.-H. Zhou, X.-T. Wu and Q.-L. Zhu, *Appl. Catal. B: Environ.*, 2022, **316**, 121667.
30. H. Zhang, Y. Wang, X. Li, K. Deng, H. Yu, Y. Xu, H. Wang, Z. Wang and L. Wang, *Appl. Catal. B: Environ.*, 2024, **340**, 123236.
31. H. Zhou, Y. Ren, Z. Li, M. Xu, Y. Wang, R. Ge, X. Kong, L. Zheng and H. Duan, *Nat. Commun.*, 2021, **12**, 4679.
32. F. Liu, X. Gao, R. Shi, Z. Guo, E. C. M. Tse and Y. Chen, *Angew. Chem. Int. Ed.*, 2023, **62**, e202300094.
33. W.-J. Liu, Z. Xu, D. Zhao, X.-Q. Pan, H.-C. Li, X. Hu, Z.-Y. Fan, W.-K. Wang, G.-H. Zhao and S. Jin, *Nat. Commun.*, 2020, **11**, 265.
34. T. Uekert, C. M. Pichler, T. Schubert and E. Reisner, *Nat. Sustain.*, 2021, **4**, 383-391.
35. A. Paulillo, M. Pucciarelli, F. Grimaldi and P. Lettieri, *Green Chem.*, 2021, **23**, 6639-6651.
36. J. Xia, J. Xu, B. Yu, X. Liang, Z. Qiu, H. Li, H. Feng, Y. Li, Y. Cai and H. Wei, *Angew. Chem.*, e202412740.
37. W. R. Leow, Y. Lum, A. Ozden, Y. Wang, D.-H. Nam, B. Chen, J. Wicks, T.-T. Zhuang, F. Li and D. Sinton, *Science*, 2020, **368**, 1228-1233.
38. H. Shin, K. U. Hansen and F. Jiao, *Nat. Sustain.*, 2021, **4**, 911-919.
39. Y. Lum, J. E. Huang, Z. Wang, M. Luo, D.-H. Nam, W. R. Leow, B. Chen, J. Wicks, Y. C. Li and Y. Wang, *Nat. Catal.*, 2020, **3**, 14-22.
40. S. Kang, X. Guo, D. Xing, W. Yuan, J. Shang, V. Nicolosi, N. Zhang and B. Qiu, *Small*, 2024, 2406068.
41. M. Jouny, W. Luc and F. Jiao, *Ind. Eng. Chem. Res.*, 2018, **57**, 2165-2177.
42. J. Qi, Y. Du, Q. Yang, N. Jiang, J. Li, Y. Ma, Y. Ma, X. Zhao and J. Qiu, *Nat. Commun.*, 2023, **14**, 6263.